Supplementary Information

An extracellular vesicle microRNA-initiated 3D DNAzyme motor for colorectal cancer diagnosis

Qian Fan [a, b], *Xu-Hong Sun* [a], *Na Wu* [a, d], *Yuan-He Wang* [c*], *Jian-Hua Wang* [a], *Ting Yang* [a*]

[a] Research Center for Analytical Sciences, Department of Chemistry, College of Sciences, Northeastern University, Box 332, Shenyang 110819, China

[b] Institute of Molecular Medicine, Renji Hospital, School of Medicine, Shanghai Jiao Tong University, Shanghai 200127, China

[c] Department of Gastrointestinal Cancer, Liaoning Cancer Hospital & Institute, Cancer Hospital of China Medical University, Shenyang 110042, China

[d] Institute of Precision Medicine, Fujian Medical University, Fujian 350004, China

*Corresponding author:

E–mail address: yangting@mail.neu.edu.cn (T. Yang), wangyuanhe@sina.com (Y-H. Wang)

Tel: +86 24 83688944; Fax: +86 24 83676698

Table of contents

Supporting Figures and Tables

Supporting Figures and Tables

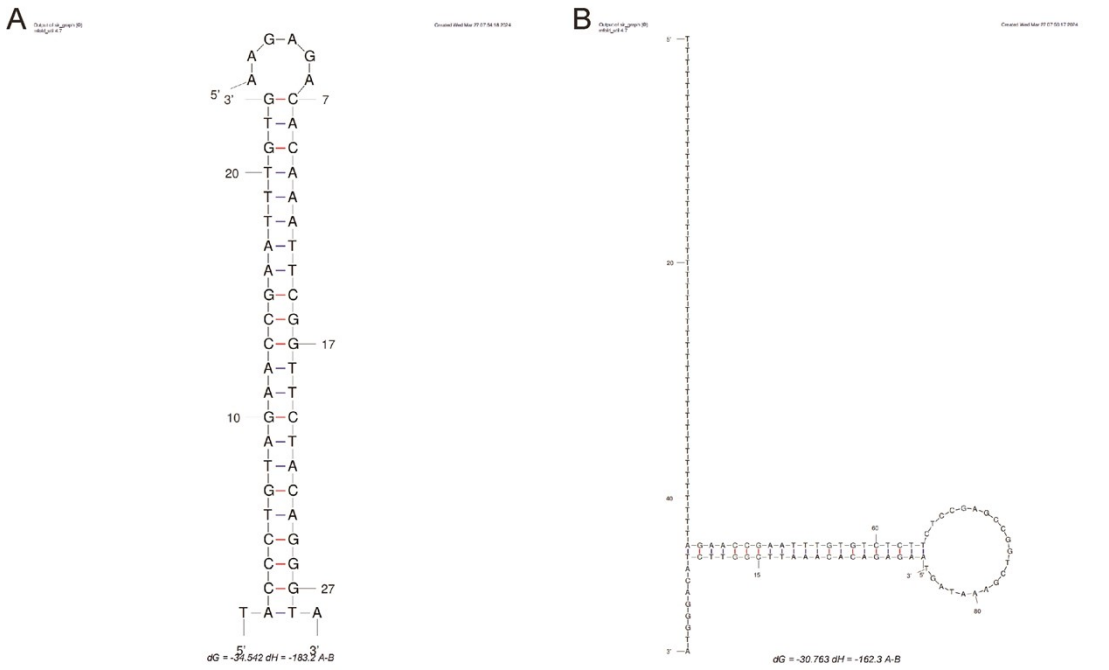

Fig. S1 The analysis results of strand hybridization generated by the UNAFold Web Server. (A) Strand hybridization between target miRNA-10b and locking-10b. (B) Strand hybridization between DNAzyme-10b and locking-10b.

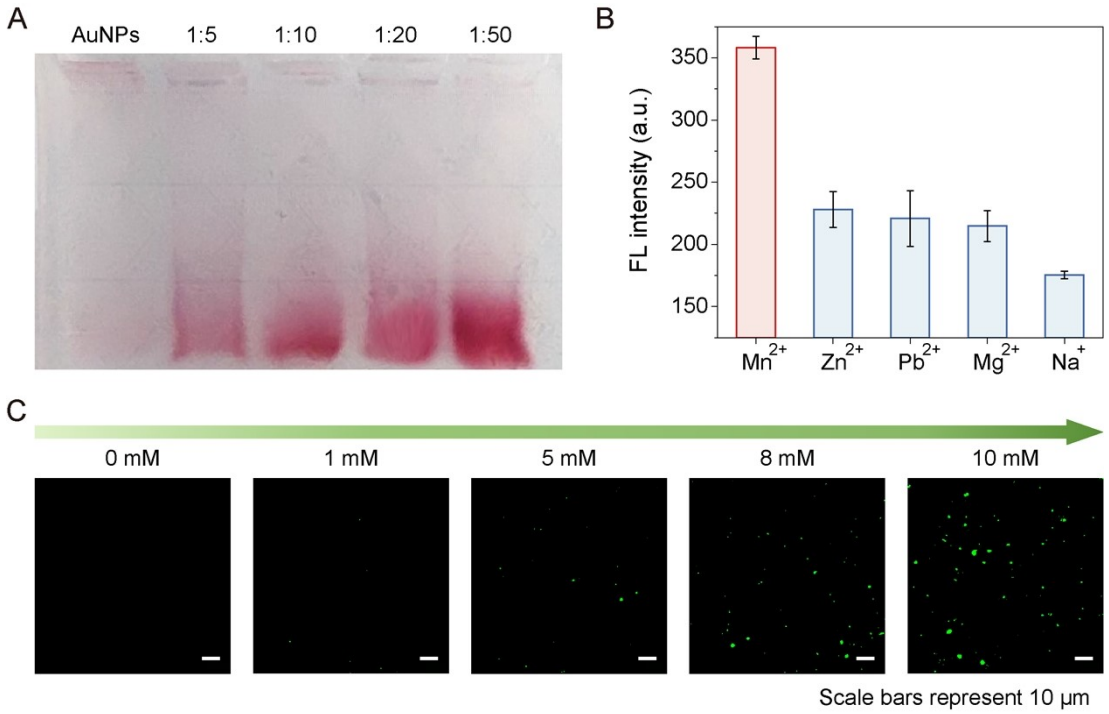

Fig. S2 Optimization of experimental conditions. (A) Agarose gel electrophoresis results of composites synthesized by DNAzyme strands and substrate strands at the

ratios of 1:5, 1:10, 1:20, and 1:50. (B) Catalytic effect of the DNAzyme motors with different auxiliary metal ions. (C) Detection effect of the system with different concentrations of Mn^{2+} as auxiliary metal ions.

In the concentration ratio optimization of DNAzyme strands and substrate strands, $n_{DNAzyme}$: $n_{substrate}$ = 1:10 was chosen because the products synthesized at 1:10 had the most uniform size and electric charge, and less tendency to aggregate, which made it easier for preparation and more suitable for the walking of DNAzyme strands with less spatial resistance to amplify signals efficiently. For catalytic effect comparison, in the presence of 500 pM miRNA-10b target sequences, different metal ions as cofactors at the same concentration brought different catalytic efficiencies, Mn^{2+}>Zn^{2+}>Pb^{2+}>Mg^{2+}>Na^{+}. For the concentration optimization of auxiliary metal ions, we tested the fluorescence signals of the systems containing 0 mM, 1 mM, 5 mM, 8 mM, 10 mM, 12 mM and 15 mM Mn^{2+}. As the concentration of Mn^{2+} increased, the fluorescent points became more numerous. And 10 mM Mn^{2+} provided the most motivation for the system and generated the most fluorescent fragments among them within the same time. The consideration of Mn^{2+} concentrations above 10 mM was abandoned, as it was experimentally found that excessive metal ions would lead to agglomeration and sedimentation of the composites in solution.

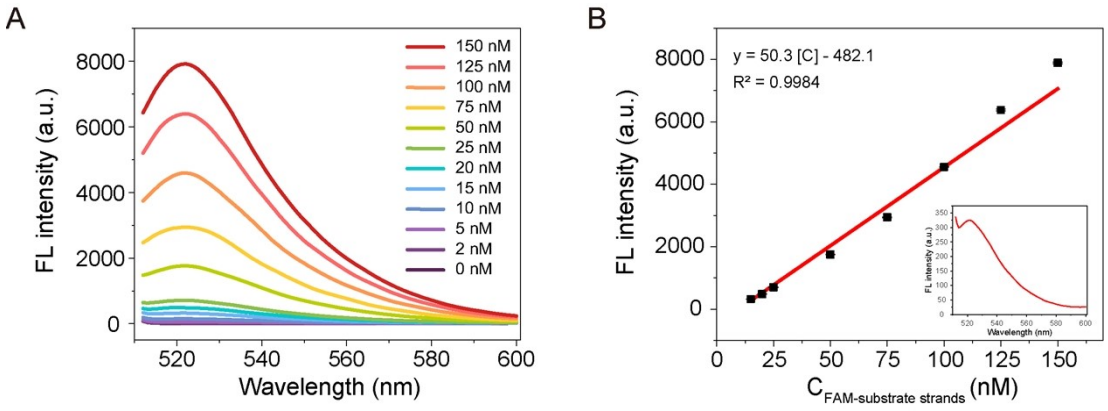

Fig. S3 Quantification of the average number of substrate strands on each AuNPs. (A) Fluorescence spectra of FAM labelled substrate strands at different concentrations. (B) Standard linear calibration curve of FAM labeled substrate strands (The inserted data graph is the fluorescence spectrum of the substrate strands released

from the DNAzyme motors after DTT treatment).

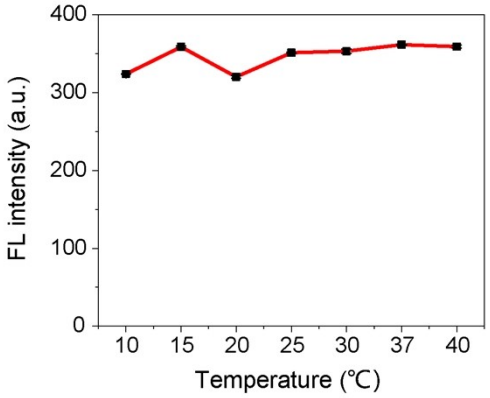

Fig. S4 Effect of temperature on the catalytic activity of the DNAzyme motor. The small differences between the fluorescence signals at 518 nm all triggered by 500 pM target miRNA-10b at different temperatures indicated the stability of DNAzyme activity in the system.

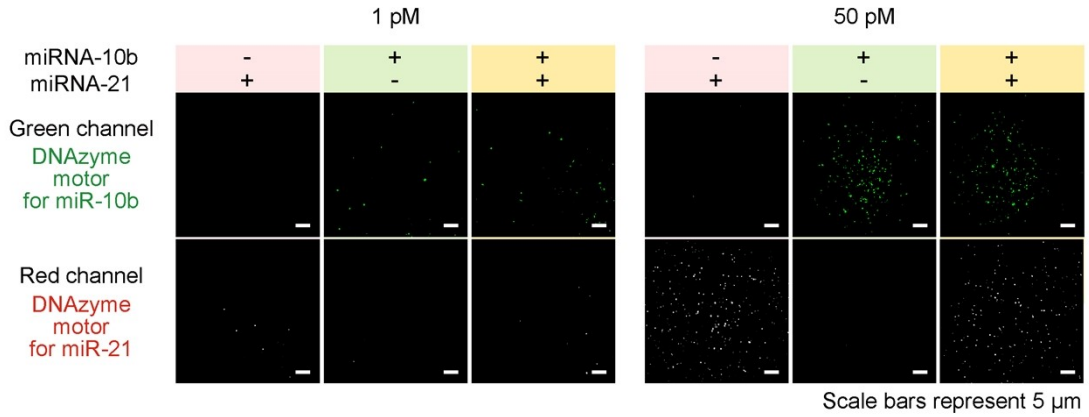

Fig. S5 Simultaneous detection of dual target miRNAs (1 pM and 50 pM). Scale bars represent 5 μm.

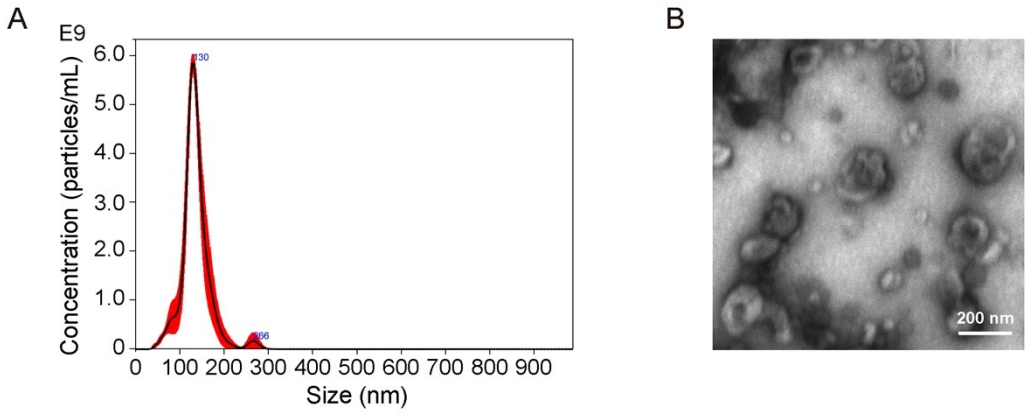

Fig. S6 Characterization of EVs isolated from blood samples of healthy donors. (A) nanoparticle tracking analysis (NTA), (B) transmission electron microscope (TEM) characterization, scale bar represents 200 nm.

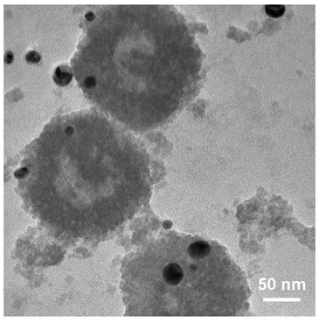

Fig. S7 TEM characterization of the separated blood-derived EVs and the DNAzyme motors entering EVs via endocytosis. Scale bar represents 50 nm. The AuNPs-DNAzyme composites were able to enter the EVs with a particle size of approximately 160 nm, and remained dispersed in them.

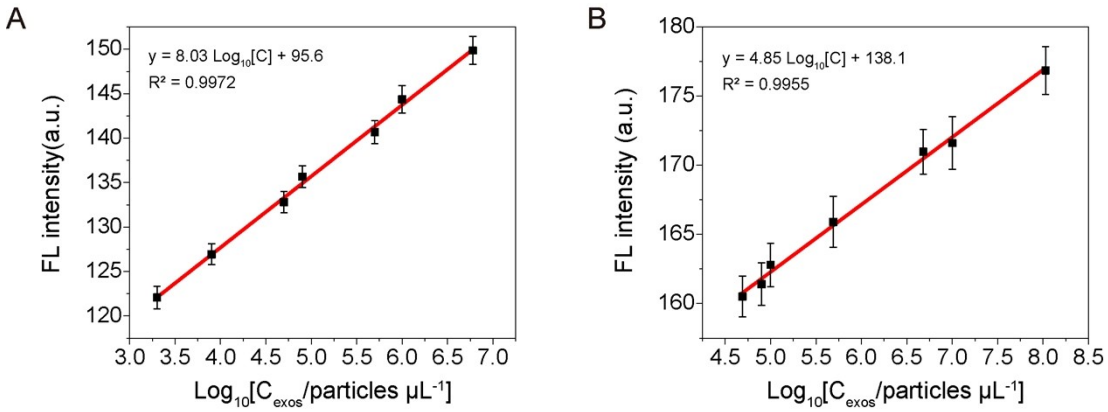

Fig. S8 Standard regression curves of EV-derived miRNA-10b detection. The miRNA-10b targets were detected by incubating the DNAzyme motors (A) within

EVs via endocytosis, and (B) in external environment with the RNA extracted from EVs. According to the results of fluorescence spectrophotometer, the latter fluorescence intensity is about 0.19 times higher overall than the former.

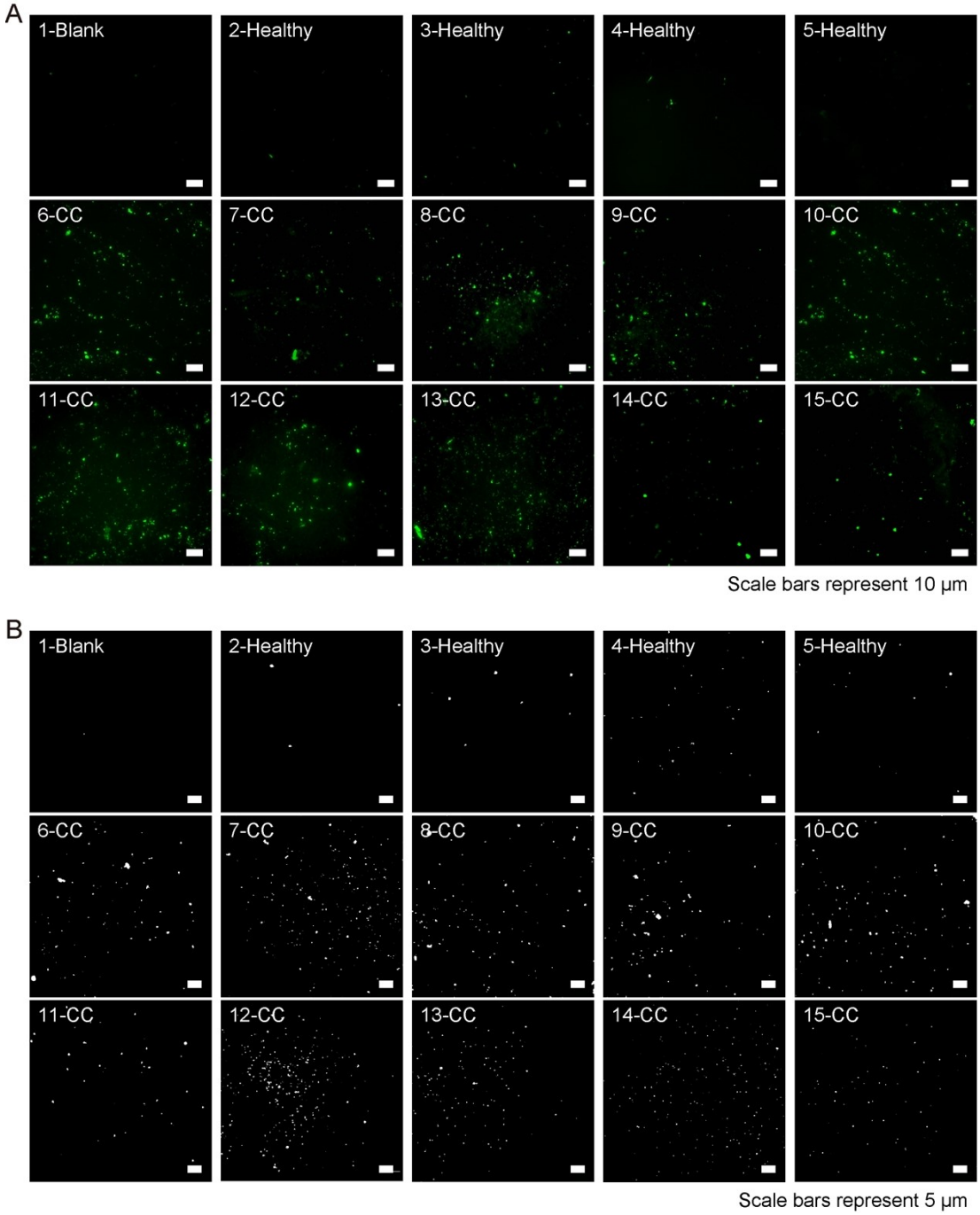

Fig. S9 Single molecule fluorescence imaging of (A) miRNA-10b and (B) miRNA-21 in the EVs from clinical samples. Five images were collected for each sample, and one of them was selected as a representative and displayed. Among them, the first image is the blank control group, images 2-15 correspond to the samples of healthy

donors, and images 6-15 correspond to the samples of colorectal cancer patients.

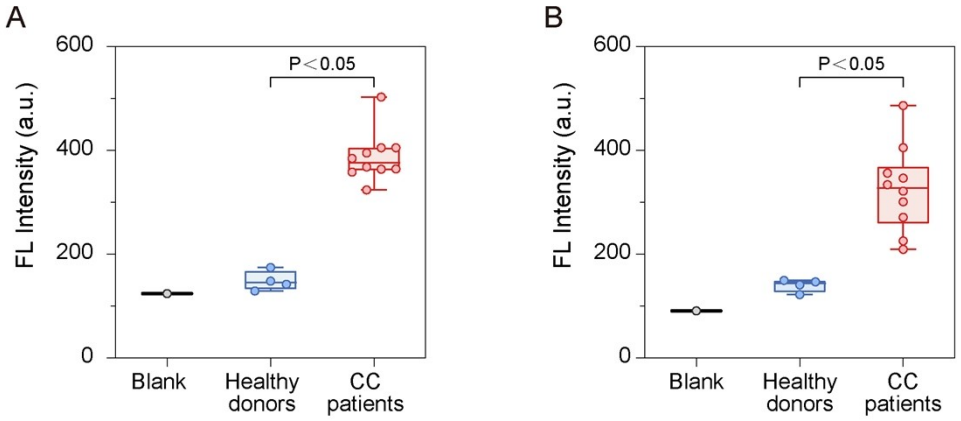

Fig. S10 The fluorescence intensity generated by DNAzyme motors initiated by (A) miRNA-10b and (B) miRNA-21 in the EVs from clinical samples.

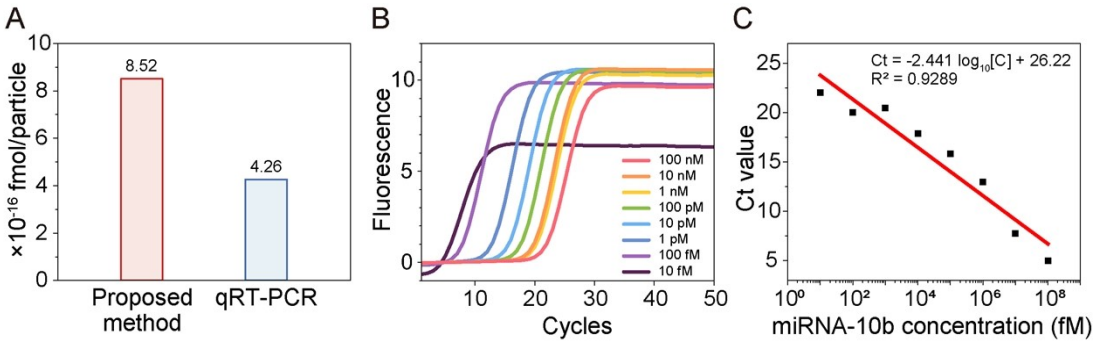

Fig. S11 Quantification of miRNA-10b in healthy donor-derived EVs by the proposed method and qPCR. (A) Comparison of results between the two methods. (B) Representative standard amplification curves of qPCR. (C) Standard curve of qPCR.

Table S1 Oligonucleotide sequences used in this study.

Oligonucleotides	Sequences（5'→3'）
Substrate-10b	HS-TTT TTT TTT TTT TTC ACT AT/rA/GGA AGA GAT-FAM
Locking-10b	AAG AGA CAC AAA TTC GGT TCT ACA GGG TA
Target miRNA-10b	UAC CCU GUA GAA CCG AAU UUG UG
DNAzyme-10b	HS-$(T)_{42}$TAG AAC CGA ATT TGT GTC TCT TCT CCG AGC CGG TCG AAA TAG T
Mis-1	TAC ACT GTA GAA CCG AAT TTG TG
Mis-2	TAC CCT GTA GAA CCG AAT TTT TG
Mis-3	TAC CCT GTA GAA GCG AAT TTG TG
Substrate-21	HS-TTT TTT TTT TCG ATC TCC TAT/rA/GGA AGT TCC GCC-Cy3
Locking-21	TTC CGC CTC AAC ATC AGT CTG ATA AGC TA
Target miRNA-21	UAG CUU AUC AGA CUG AUG UUG A
DNAzyme-21	HS-$(T)_{43}$GAC TGA TGT TGA GGC GGA ACC AGG TCA AAG GTG GGT GAG GGG ACG CCA AGA GTC CCC GCG GTT AGG AGA TCG
Mis-4	TAG CTT ATC ACA CTG ATG CTG A
Mis-5	TAG CTC ATC AGA ATG ATG TCG A
Mis-6	TAG CGT AGT ATA CAG AAG TCC A
RT-Primer-10b	GTC GTA TCC AGT GCA GGG TCC GAG GTA TTC GCA CTG GAT ACG ACC ACA AA
Primer-10b	CGC GTA CCC TGT AGA ACC GAA
Universal Primer	AGT GCA GGG TCC GAG GTA TT

Table S2 Patient information of clinical samples.

ID	Age	Gender	Disease type and staging
2	44	female	Colon cancer, stage IV
3	71	male	Right colon cancer, stage IV
4	63	female	Rectal Cancer, stage IV
5	55	male	Colon cancer, stage IV
6	54	male	Sigmoid colon cancer, stage IV
7	31	female	Sigmoid colon cancer, stage IV
8	70	male	Sigmoid colon cancer, stage IV
9	59	male	Sigmoid colon cancer, stage IV
10	48	male	Rectal Cancer, stage IV
11	68	male	Sigmoid colon cancer, stage IV
12	25	male	Healthy control
13	26	male	Healthy control
14	25	male	Healthy control
15	29	male	Healthy control